17th Australasian Fluid Mechanics Conference
Auckland, New Zealand
5-9 December 2010

Impact of resolution on stochastic subgrid parameterisations for atmospheric flows

V. Kitsios[1], J. S. Frederiksen[1] and M. J. Zidikheri[2]

[1]Centre for Australian Weather and Climate Research,
CSIRO Marine and Atmospheric Research, Aspendale 3195, AUSTRALIA

[2]Centre for Australian Weather and Climate Research,
Australian Bureau of Meteorology, Melbourne 3001, AUSTRALIA

Abstract

A stochastic spectral subgrid model for the Large Eddy Simulation (LES) of a quasi-geostrophic atmospheric flow is presented, with particular focus on the influence of resolution. The approach of Frederiksen & Kepert [3] is adopted, where the subgrid scales are represented by a drain-dissipation matrix plus a stochastic backscatter term. Two LES variants are presented: an anisotropic parameterisation, in which the subgrid model is dependent on the zonal and total wavenumbers; and an isotropic parameterisation only dependent on the total wavenumbers. The terms required for the subgrid parameterisations are determined from higher resolution Direct Numerical Simulations (DNSs). Two DNSs are presented, one with 126 zonal and total wavenumbers, and a second with 252 wavenumbers. The LES simulations have half the wavenumbers as compared to the respective DNS data sets. For both resolutions the LES variants agree with the kinetic energy spectra from the DNS very well. As the LES resolution increases the subgrid eddy viscosity and stochastic backscatter both decrease.

Introduction

With the current level of computer hardware technology, it is not possible in a reasonable amount of time to simulate the atmosphere or ocean by resolving all of the scales of motion. In geophysical fluid dynamics a DNS is understood to be a highly resolved simulation with hyper-viscosity terms accounting for the unresolved scales. In a LES the large structures are resolved and the remaining small scales are approximated by a subgrid parameterisation. The first such parameterisation was the Smagorinsky eddy viscosity model [8], in which the subgrid scales were related to the local strain rate via a single specified parameter. The next major development in this area was the Dynamic Smagorinsky model of Germano et. al. [4], where the eddy viscosity was calculated from the scales resolved in a test filter at each time step. Both of these models rely on a deterministic relationship between the resolved and subgrid scales of motion. A stochastic version of the Smagorinsky model was the first proposed by Leith [6].

With application to barotropic atmospheric flows, Frederiksen & Davies [2] and Frederiksen [1] developed a turbulence closure with wavenumber-dependent dissipation (related to the eddy viscosity) and stochastic backscatter terms, with no specified parameters needed. In an effort to widen the applicability of the closure, Frederiksen & Kepert [3] developed a means by which the dissipation and stochastic backscatter terms could be determined from a reference DNS data set. This is the approach adopted here. The present study specifically builds upon the work of Zidikheri & Frederiksen [9], analysing a baroclinic atmospheric flow configuration. In Zidikheri & Frederiksen [9] one DNS was performed with 126 wavenumbers, and LES simulations were undertaken with truncation wavenumbers of 63 and 31. In the present study two DNS data sets are produced with truncation wavenumbers of 252 and 126. LES simulations associated with each DNS data set are performed such that the LES truncation wavenumber is half of the respective DNS truncation wavenumber. This will illustrate how the subgrid parameterisation changes with resolution.

The paper is organised as follows. In the following section the quasi-geostrophic potential vorticity equation (QGPVE) is outlined, which is solved to generate the DNS data sets. The LES version of the QGPVE is then presented, along with the details surrounding the stochastic modelling of the subgrid scales. The kinetic energy spectra from the DNS are then compared to the spectra from both anisotropic and isotropic variants of the LES.

Direct Numerical Simulation of the Baroclinic Quasi-Geostrophic Equations

The numerical integration of the QGPVE is a useful and relatively computationally inexpensive means of simulating atmospheric flows. The equation is derived on the basis of approximate geostrophic balance, which is the balance between the pressure gradient and Coriolis forces. The QGPVE is derived from the variable density form of the Navier-Stokes equations (NSE) in spherical coordinates, and subject to rotation. The thickness of the atmosphere is thin in comparison with the radius of the Earth, and the vertical velocity (w) is small in comparison to the zonal (u) and meridional (v) velocities. This allows one to represent the horizontal flow field by the streamfunction ψ. Assuming that the flow is in hydrostatic balance, $\partial p/\partial z = -\rho g$, where ρ is a stratified density, and g is the gravitational constant. This relationship allows one to replace the vertical coordinate z, with a pressure coordinate p. In the present study two discrete vertical levels are used with $j = 1$ representing the upper level at 250hPa ($z \approx 10.4$km), and $j = 2$ the lower level at 750hPa ($z \approx 2.5$km). This model captures the important mechanisms of barotropic and baroclinic instabilities.

The field variables are non-dimensionalised by the radius of the Earth ($a = 6371$km) as a length scale, and the inverse of the Earth's angular velocity ($\Omega = 7.292 \times 10^{-5}\text{s}^{-1}$) as a time scale. They are expanded into spherical harmonics with zonal (longitudinal) wavenumber m, and total wavenumber n. Note the latitudinal (meridional) wavenumber is $n-m$. For convenience, instead of solving for the streamfunction, one solves for the reduced potential vorticity spectral coefficients,

$$q^j_{mn} = \zeta^j_{mn} + (-1)^j F_L \left(\psi^1_{mn} - \psi^2_{mn}\right) , \qquad (1)$$

where the superscript j on the flow variables denotes the level, and $\zeta^j_{mn} = -n(n+1)\psi^j_{mn}$ are the spectral coefficients of the vorticity. F_L is a layer coupling parameter, which is inversely proportional to the temperature difference between the two levels, and related to the Rossby radius of deformation by $r_{\text{Ros}} = 1/\sqrt{2F_L}$. The evolution of q^j_{mn} is then given by

$$\frac{\partial q^j_{mn}}{\partial t} = \mathrm{i}\sum_{pq}\sum_{rs} K^{mpr}_{nqs}\psi^j_{-pq}q^j_{-rs} + \kappa(\tilde{q}^j_{mn} - q^j_{mn}) - D^j_0(m,n)\zeta^j_{mn} , \qquad (2)$$

where, the summations are over the triangular truncated wavenumber set

$$\mathbf{T} = [\ p,q,r,s\ |\ -T \le p \le T\ ,\ |p| \le q \le T\ ,\\ -T \le r \le T\ ,\ |r| \le s \le T\ ]\ , \tag{3}$$

with T the DNS truncation wavenumber. K^{mpr}_{nqs} are the interaction coefficients given by

$$K^{mpr}_{nqs} = \int_{-1}^{1} P^m_n \left(pP^p_q \frac{dP^r_s}{d\mu} - rP^r_s \frac{dP^p_q}{d\mu} \right) d\mu\ , \tag{4}$$

where $P^m_n(\mu)$ are the orthonormal Legendre functions [2]. Since we assign $P^{-m}_n = P^m_n$, this means $q^j_{-rs} = q^{j*}_{rs}$ and $\psi^j_{-pq} = \psi^{j*}_{pq}$, and the superscript $*$ is the complex conjugate operation. Also $\dagger$ denotes the Hermitian conjugate for vectors and matrices. $\tilde{q}^j_{mn}$ is the climate to which the model is driven, via the relaxation parameter κ. The bare dissipation operator

$$D^j_0(m,n) = \alpha^j + \nu^j_0[n(n+1)]^4 + \mathrm{i}\omega_{mn}\ , \tag{5}$$

where $\omega_{mn} = -Bm/(n(n+1))$ is the the Rossby wave frequency, and B the Coriolis parameter. Under the chosen non-dimensionalisation $B = 2$. α^j are the drag terms, and ν^j_0 are the hyper-viscosities, which account for the unresolved scales in the DNS.

The values of α^j and ν^j_0 are selected so that in the inertial range the log of kinetic energy decreases with the log of the wavenumber according to an approximate linear gradient of -3, to be representative of two-dimensional turbulence [5]. This approach is deemed adequate as the resolved horizontal scales of motion are large in comparison to the vertical domain size. In addition, according to the measurements of [7] the $-5/3$ logarithmic gradient associated with three-dimensional turbulence is observed at wavelengths less than 300km. In the present study only the smallest resolved wavelength of approximately 160km is within this range.

The time integration of (2), produces the data required to determine the subgrid dissipation and backscatter terms necessary for the LES. Details on this procedure are presented in the following section.

Stochastic modelling of the subgrid scales in the Large Eddy Simulations

The LES is truncated further as compared to the DNS, with the wavenumbers confined to the set

$$\mathbf{R} = [\ p,q,r,s\ |\ -T_R \le p \le T_R\ ,\ |p| \le q \le T_R\ ,\\ -T_R \le r \le T_R\ ,\ |r| \le s \le T_R\ ]\ , \tag{6}$$

where T_R is the LES truncation wavenumber and $T_R < T$. The subgrid wavenumber set can then be defined as $\mathbf{S} = \mathbf{T} - \mathbf{R}$. To facilitate a discussion on the decomposition of these scales of motion, for a given wavenumber pair we let $\mathbf{q}$ equal the transpose of (q^1_{mn}, q^2_{mn}). This vector notation allows one to express

$$\mathbf{q}_t(t) = \mathbf{q^R}_t(t) + \mathbf{q^S}_t(t)\ , \tag{7}$$

where $\mathbf{q}_t$ is the tendency (or time derivative) of $\mathbf{q}$. $\mathbf{q^R}_t$ is the tendency of the resolved scales where all triadic interactions involve wavenumbers less than T_R, and consequently no parameterisation is required. $\mathbf{q^S}_t$ is the remaining subgrid tendency in which at least one wavenumber component involved in the triadic interactions is greater than T_R. It is the latter tendency that must be modelled.

The subgrid tendency can be further decomposed such that

$$\mathbf{q^S}_t(t) = \overline{\mathbf{f}} + \widehat{\mathbf{q}}^{\mathbf{S}}_t(t)\ , \tag{8}$$

where $\overline{\mathbf{f}} \equiv \overline{\mathbf{q^S}_t}$ is the time averaged subgrid tendency, and $\widehat{\mathbf{q}}^{\mathbf{S}}_t$ the fluctuating component. In the present study $\overline{\mathbf{f}}$ is determined directly from the DNS data, and the fluctuating component is represented by the stochastic equation

$$\widehat{\mathbf{q}}^{\mathbf{S}}_t(t) = -\mathbf{D_d}\ \widehat{\mathbf{q}}(t) + \widehat{\mathbf{f}}(t)\ , \tag{9}$$

where $\mathbf{D_d}$ is the subgrid drain dissipation matrix, $\widehat{\mathbf{q}}$ is the fluctuating component of $\mathbf{q}$, and $\widehat{\mathbf{f}}$ is a random forcing vector. Again as the present simulations have two vertical levels, for a given wavenumber pair $\mathbf{D_d}$ is a time independent 2×2 matrix, and $\widehat{\mathbf{f}}$ is a time dependent 2 element column vector.

After some manipulation of (9), $\mathbf{D_d}$ is determined by evaluating

$$\mathbf{D_d} = -\left\langle \int_{t_0}^{t} \widehat{\mathbf{q}}^{\mathbf{S}}_t(\sigma)\widehat{\mathbf{q}}^{\dagger}(t_0)d\sigma \right\rangle \left\langle \int_{t_0}^{t} \widehat{\mathbf{q}}(\sigma)\widehat{\mathbf{q}}^{\dagger}(t_0)d\sigma \right\rangle^{-1}. \tag{10}$$

The angled brackets denote ensemble averaging, with each ensemble member determined by shifting the initial time t_0 and the final time $t = t_0 + \tau$ forward by one timestep. τ is chosen to capture the average subgrid contribution to the resolved scales.

The model of the stochastic backscatter term $\widehat{\mathbf{f}}$ is determined by first calculating the non-linear noise covariance matrix given by

$$\mathbf{F} = \left\langle \widehat{\mathbf{f}}(t)\ \widehat{\mathbf{q}}^{\dagger}(t) \right\rangle + \left\langle \widehat{\mathbf{q}}(t)\ \widehat{\mathbf{f}}^{\dagger}(t) \right\rangle\ . \tag{11}$$

By again manipulating (9), $\mathbf{F}$ can be determined from

$$\left\langle \widehat{\mathbf{q}}^{\mathbf{S}}_t(t)\ \widehat{\mathbf{q}}^{\dagger}(t) \right\rangle + \left\langle \widehat{\mathbf{q}}(t)\ \widehat{\mathbf{q}}^{\mathbf{S}\dagger}_t(t) \right\rangle = \\ -\mathbf{D_d}\ \left\langle \widehat{\mathbf{q}}(t)\ \widehat{\mathbf{q}}^{\dagger}(t) \right\rangle - \left\langle \widehat{\mathbf{q}}(t)\ \widehat{\mathbf{q}}^{\dagger}(t) \right\rangle\ \mathbf{D_d}^{\dagger} + \mathbf{F}\ , \tag{12}$$

given that $\mathbf{D_d}$ has been previously calculated. It is clear from (12) that $\mathbf{F}$ is Hermitian, which by definition has real eigenvalues and can be decomposed into

$$\mathbf{F} = \mathbf{P} \begin{bmatrix} \lambda_1 & 0 \\ 0 & \lambda_2 \end{bmatrix} \mathbf{P}^{\dagger}\ , \tag{13}$$

where λ_1 and λ_2 are the eigenvalues of $\mathbf{F}$, and $\mathbf{P}$ is a unitary matrix whose columns consist of the associated eigenvectors. The instantaneous values of $\widehat{\mathbf{f}}$ are now related to the eigenvalues and eigenvectors of $\mathbf{F}$. First we assume that $\widehat{\mathbf{f}}$ is a white noise process such that

$$\left\langle \widehat{\mathbf{f}}(t)\ \widehat{\mathbf{f}}^{\dagger}(t') \right\rangle = \mathbf{F}\ \delta(t-t')\ , \tag{14}$$

the discrete time form of which is

$$\left\langle \widehat{\mathbf{f}}(t)\ \widehat{\mathbf{f}}^{\dagger}(t') \right\rangle = \mathbf{F}\ \frac{1}{2\Delta t}\ , \tag{15}$$

where $\Delta t = t' - t$ is the time step size. Using the eigenvalue decomposition in (13) one can then express the instantaneous values of $\widehat{\mathbf{f}}$ by

$$\widehat{\mathbf{f}}(t) = \frac{1}{\sqrt{2\Delta t}} \mathbf{P} \begin{pmatrix} \sqrt{\lambda_1}\, r_1(t) \\ \sqrt{\lambda_2}\, r_2(t) \end{pmatrix}\ , \tag{16}$$

where r_1 and r_2 are standard random numbers with Gaussian distributions. Importantly the proposed form of $\widehat{\mathbf{f}}$ in (16) satisfies (15). The eigenvalues, however, can sometimes be less

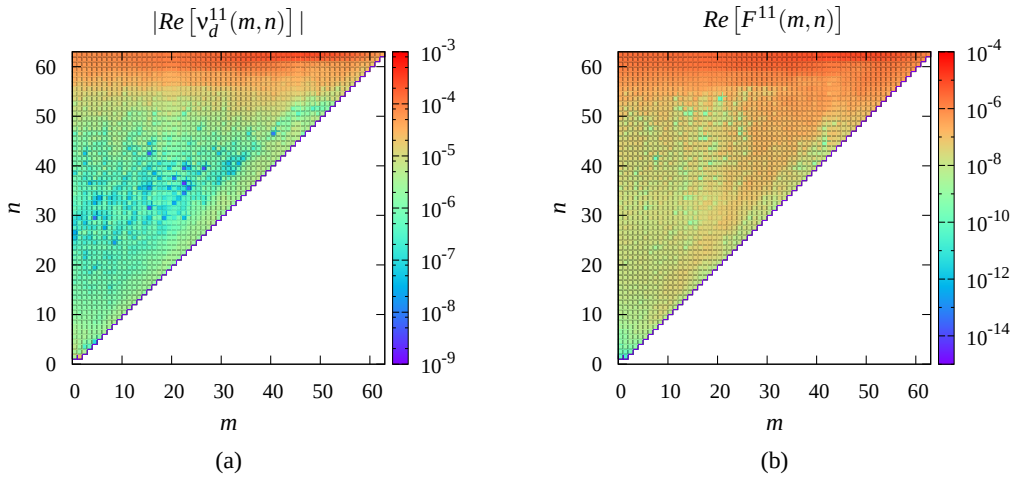

Figure 1: Anisotropic subgrid coefficients for the $T126$ data set: (a) $|Re\left[\nu_d^{11}(m,n)\right]|$; and (b) $Re\left[F^{11}(m,n)\right]$.

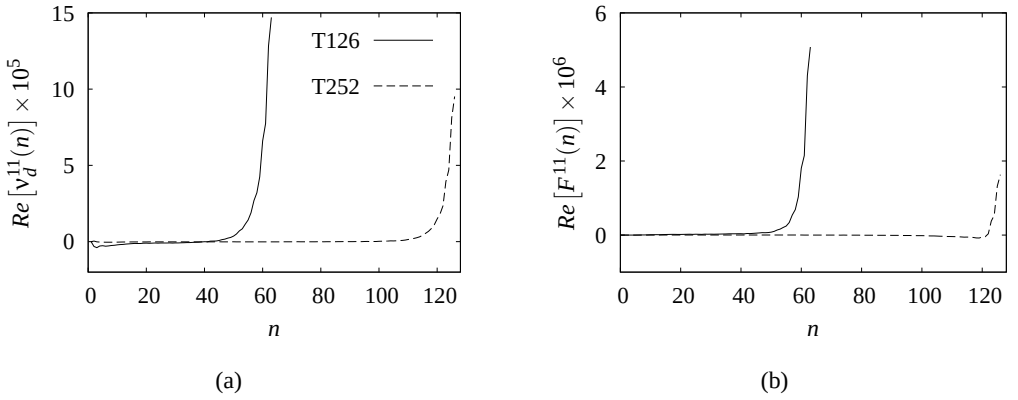

Figure 2: Isotropic subgrid coefficients: (a) $Re\left[\nu_d^{11}(n)\right]$; and (b) $Re\left[F^{11}(n)\right]$. The legend in (a) is applicable to both figures.

than zero due to sampling error. In this case, a cut-off total wavenumber n_c is defined as the highest total wavenumber with non-negative eigenvalues for all m. For all wavenumber pairs with $n < n_c$, $\widehat{\mathbf{f}}$ is set to zero and the associated values of $\mathbf{D_d}$ are replaced with those of the net dissipation

$$\mathbf{D_n} = -\left\langle \widehat{\mathbf{q}^S}_t(t)\,\widehat{\mathbf{q}}^\dagger(t)\right\rangle \left\langle \widehat{\mathbf{q}}(t)\,\widehat{\mathbf{q}}^\dagger(t)\right\rangle^{-1} \quad . \tag{17}$$

Note the eddy viscosity is related to the dissipation via the expression $\boldsymbol{\nu_d}(m,n) = \mathbf{D_d}(m,n)/(n(n+1))$.

Finally the equation solved for the anisotropic LES is

$$\begin{aligned}\frac{\partial q^j_{mn}}{\partial t} &= \mathrm{i}\sum_{pq}\sum_{rs} K^{mpr}_{nqs}\,\psi^j_{-pq}q^j_{-rs} + \kappa(\tilde{q}^j_{mn} - q^j_{mn}) - D^j_0(m,n)\zeta^j_{mn} \\ &- \sum_{l=1}^{2} D^{jl}_d(m,n)\,\hat{q}^l_{mn} + \hat{f}^j_{mn} + \overline{f}^j_{mn}\,,\end{aligned} \tag{18}$$

over the wavenumber set $\mathbf{R}$. As presented in (18), each wavenumber pair has a unique $\mathbf{D_d}$ and $\widehat{\mathbf{f}}$. For the isotropic LES, the matrices $\mathbf{D_d}$ and $\mathbf{F}$ are averaged over the zonal wavenumbers m, so that they are now only functions of the total wavenumbers n. The isotropic eigenvalues are then calculated from the m averaged $\mathbf{F}$ matrix, and the random forcing function is consequently only dependent on n. The isotropised versions of $\mathbf{D_d}$ and $\mathbf{F}$ are presented in the following section.

Results

Two resolution cases are analysed denoted by $T126$ and $T252$, referring to the DNS truncation wavenumber T listed in table 1. The dissipation and stochastic backscatter terms required to perform the LES are derived from these data sets. Anisotropic and isotropic subgrid scale models are undertaken, with the LES truncation wavenumber T_R also listed in table 1. For a given case, the same Δt and the number of time steps (N_t) are used for the DNS and LES variants to provide a direct comparison between the kinetic energy spectra accumulated over the time period. In all cases the simulations are driven toward $\tilde{q}^j_{mn}$ with a the relaxation parameter of $\kappa = 10^{-6}\mathrm{s}^{-1}$. $\tilde{q}^j_{mn}$ consists of two large easterly moving jets; one in the mid latitudes of each hemisphere. Further details on the structure of $\tilde{q}^j_{mn}$ can be found in [9]. To be representative of atmospheric flows the layer coupling parameter in SI units is $F_L = 2.5\times10^{-12}\mathrm{m}^{-2}$, with $r_{\mathrm{Ros}} = 4.47\times10^5\mathrm{m}$ and a wavelength of $2\pi r_{\mathrm{Ros}} = 2.81\times10^6\mathrm{m}$. The associated non-dimensionalised Rossby wavenumber is $k_{\mathrm{Ros}} = a/r_{\mathrm{Ros}} \approx 14$. It is clear that for all simulations presented within, the large scale Rossby waves are resolved as $k_{\mathrm{Ros}} < T_R < T$. Note ocean simulations are an order of magnitude more computationally challenging with a larger $k_{\mathrm{Ros}} \approx 140$.

The anisotropic subgrid dissipation coefficients are calculated from the DNS data using (10) with $\tau = 24\Delta t$ in all cases. For the $T126$ data set, the amplitude of the real component of eddy viscosity $\nu_d^{11}(m,n)$ is illustrated in Fig. 1(a), and the real com-

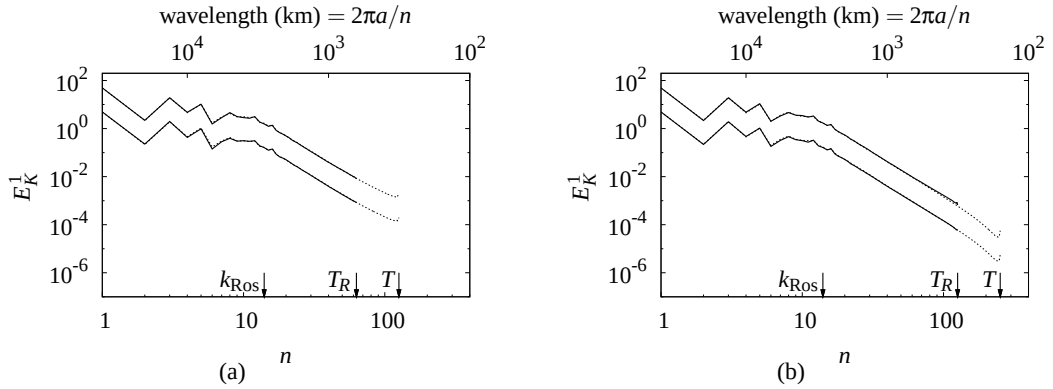

Figure 3: Comparison of the kinetic energy spectra on level 1 (E_K^1): for (a) $T126$; and (b) $T252$. The top spectra in each graph is a comparison between the DNS (dotted line) and the isotropic LES. The bottom spectra is a comparison between the DNS and anisotropic LES, with both spectra shifted down one decade for clarity.

	$T126$	$T252$
T	126	252
T_R	63	126
N_t	40000	80000
Δt (sec)	450	225

Table 1: Numerical parameters for data sets $T126$ and $T252$.

ponent of the non-linear noise covariance coefficient $F^{11}(m,n)$ is presented in Fig. 1(b). Both of these coefficients generally increase with n, and for $n > 55$ they are largely independent of m. The eddy viscosity is isotropised with $Re\left[\nu_e^{11}(n)\right]$ shown in Fig. 2(a), and exhibits a cusp like shape approaching the LES truncation wavenumber T_R. The isotropised version of the $T252$ data set is also illustrated in Fig. 2(a), with a lower maximum value at T_R. The non-linear noise covariance is isotropised with $Re\left[F^{11}(n)\right]$ illustrated in Fig. 2(b) for both the $T126$ and $T252$ data sets. This figure indicates that the magnitude of $Re\left[F^{11}(n)\right]$ also decreases with resolution.

A comparison is now made between the time and m averaged kinetic energy spectra on level 1 (E_K^1) resulting from the DNS, anisotropic LES and isotropic LES. E_K^1 is illustrated in Fig. 3(a) for $T126$ and in Fig. 3(b) for $T252$. The approximate wavenumber of the Rossby wave ($k_{\mathrm{Ros}} \approx 14$) is indicated on each graph. The appropriate DNS truncation wavenumber T, and the LES truncation wavenumber T_R are also labelled. These figures illustrate that the spectra exhibit excellent agreement at both resolutions. The level 2 spectra is not presented within; however, the agreement is equally as impressive. Typical of these types of simulations, there is an upward curve at the high wavenumber end of the DNS spectra. This feature, however, has not hindered the ability to illustrate the subgrid parameterisation process.

Concluding remarks

DNS data from a two level quasi-geostrophic atmospheric model has been compared to associated LES simulations with stochastic subgrid parameterisations. The simulations were performed at two resolutions with DNS truncated wavenumbers of 126 and 252 in the periodic directions. The associated LES simulations were performed with half the number of wavenumbers in each direction. Two LES variants were undertaken for both resolutions, an anisotropic and an isotropic closure. All of the terms required for the subgrid models were derived from the DNS data sets. The maximum values of $\nu_d^{11}(n)$ and $F^{11}(n)$ were found to decrease as resolution increased. The DNS and both LES variants had very similar kinetic energy spectra. The simpler isotropic closure is sufficient because the anisotropic coefficients in figure 1 are similar for all m at a given n. This may or may not be the case when topology is added.

The subgrid parameterisation method presented within is equally applicable to General Circulation Models, and general studies on three-dimensional turbulence.

Acknowledgements

The first author would like to acknowledge the CSIRO Office of the Chief Executive for funding his research position.

References

[1] Frederiksen, J. S., Subgrid-scale parameterizations of eddy-topographic force, eddy viscosity and stoachstic backscatter for flow over topography, *J. Atmos. Sci*, **56**, 1999, 1481–1493.

[2] Frederiksen, J. S. and Davies, A. G., Eddy viscosity and stochastic backscatter parameterizations on the sphere for atmospheric circulation models, *J. Atmos. Sci*, **54**, 1997, 2475–2492.

[3] Frederiksen, J. S. and Kepert, S. M., Dynamical subgrid-scale parameterizations from Direct Numerical Simulations, *J. Atmos. Sci.*, **63**, 2006, 3006–3019.

[4] Germano, M., Piomelli, U., Moin, P. and Cabot, W. H., A dynamic subgrid-scale eddy viscosity model, *Phys. Fluids A*, **3**, 1991, 1760–1765.

[5] Kraichnan, R., Intertial ranges in two-dimensional turbulence, *Phys. Fluids*, **10**, 1967, 1417–1423.

[6] Leith, C. E., stochastic backscatter in a subgrid-scale model: Plane shear mixing layer, *Phys. Fluids*, **2**, 1990, 297–299.

[7] Nastrom, G. D., Gage, K. S. and Jasperson, W. H., Kinetic energy spectrum of large- and mesoscale atmospheric processes, *Nature*, **310**, 1984, 36–38.

[8] Smagorinsky, J., General circulation experiments with the primitive equations: I. the basic experiment, *Monthly Weather Review*, **91**, 1963, 99–164.

[9] Zidikheri, M. J. and Frederiksen, J. S., Stochastic subgrid parameterizations for simulations of atmospheric baroclinic flows, *J. Atmos. Sci.*, **66**, 2009, 2844–2858.